Changes in the Distribution of Rain Frequency and Intensity in Response to Global Warming*

ANGELINE G. PENDERGRASS AND DENNIS L. HARTMANN

Department of Atmospheric Sciences, University of Washington, Seattle, Washington

(Manuscript received 6 March 2014, in final form 23 July 2014)

ABSTRACT

Changes in the frequency and intensity of rainfall are an important potential impact of climate change. Two modes of change, a shift and an increase, are applied to simulations of global warming with models from phase 5 of the Coupled Model Intercomparison Project (CMIP5). The response to CO_2 doubling in the multimodel mean of CMIP5 daily rainfall is characterized by an increase of 1% K^{-1} at all rain rates and a shift to higher rain rates of 3.3% K^{-1}. In addition to these increase and shift modes of change, some models also show a substantial increase in rainfall at the highest rain rates called the extreme mode of response to warming. In some models, this extreme mode can be shown to be associated with increases in grid-scale condensation or gridpoint storms.

1. Introduction

Rain responds to global warming in climate models in two robust ways: the total amount of rainfall increases, and the rain rates of the heaviest events increase more. The rate of increase of global-mean rainfall is constrained by energetics to roughly 2% K^{-1} (Held and Soden 2006), while the intensity of extreme events is driven by increases in moisture (specifically moisture convergence) and increases by at least 5.5% K^{-1} (O'Gorman and Schneider 2009) but possibly much more (Allan et al. 2010). Trenberth (1999) explained that this disparity implies a change in the frequency distribution of rainfall toward more heavy rain, as well as a decrease in rain frequency.

The energetic constraint limits changes in global-mean precipitation in models (Mitchell et al. 1987; Allen and Ingram 2002) to a rate less than the increase in water vapor with warming (Held and Soden 2006). The increase in precipitation must be less than the increase in moisture due to the radiative properties of water vapor (Stephens and Ellis 2008). The clear-sky radiative cooling response to warming, moistening, and CO_2 increase is closely related to the rate of increase of precipitation in models from phase 5 of the Coupled Model Intercomparison Project (CMIP5; Pendergrass and Hartmann 2014a).

Extreme precipitation events should be driven by moisture and its convergence, which increase with warming (Trenberth 1999). Rain rates at the highest percentiles of the distribution increase at about the same rate as water vapor in simulations from one GCM (Allen and Ingram 2002; Pall et al. 2007). Moisture convergence can be decomposed into moisture and vertical velocity (Emori and Brown 2005; Chou et al. 2012). The rate of increase of the 99.9th percentile of daily rain rate in GCMs scales with vertical moisture advection in the extratropics, but this scaling works less well in the tropics (O'Gorman and Schneider 2009; Sugiyama et al. 2010). The rate of increase of extreme precipitation events may be even greater than the increase in moisture because additional latent heating could invigorate convection, further increasing rain rates (Allan et al. 2010; Trenberth 2011).

The rest of the rain distribution also changes with warming. While the heaviest events become more frequent with warming, less-heavy events become less frequent (e.g., Sun et al. 2007; Chou et al. 2012; Lau et al. 2013). This pattern is suggestive of a shift from moderate to higher rain rates. In model simulations of global warming, the total wet-day frequency decreases while

* Supplemental information related to this paper is available at the Journals Online website: http://dx.doi.org/10.1175/JCLI-D-14-00183.s1.

Corresponding author address: Angeline G. Pendergrass, NCAR, P.O. Box 3000, Boulder, CO 80307.
E-mail: apgrass@ucar.edu

DOI: 10.1175/JCLI-D-14-00183.1

total intensity increases, but by only 2% K^{-1} (Sun et al. 2007). There is disagreement about whether the frequency of light rain events increases (Lau et al. 2013) or decreases (Chou et al. 2012) in GCM simulations.

We approach the response of the rainfall distribution from the energetic perspective. Because it is the latent heat imparted by rain rather than rain frequency that is energetically constrained, we focus on the distribution of rain amount. Energetics also motivates us to take a global perspective and integrate over large areas that will average over shifts of precipitating systems in space. This large-scale perspective also ensures that we capture the entire distribution of rain, without missing the heaviest events, which make substantial contributions to rain amount.

Atmospheric cooling is smoother in space and time than precipitation, so we expect the increased atmospheric cooling to affect the entire precipitation distribution. We anticipate coherent modes of change, where changes at any rain rate are related to those at other rain rates, so we formulate modes of response of the distribution.

The goals of this study are to describe the character of the changes in precipitation that balance increased atmospheric cooling and to quantify ways the distribution of rain could change, in order to understand how the constraints of energy and moisture are simultaneously met. In an accompanying paper (Pendergrass and Hartmann 2014b), we introduce two modes of coherent change of the rain amount distribution: an increase in rain amount at all rain rates (the increase mode) and a shift of the rain amount distribution to higher rain rates (the shift mode). The increase mode changes the total amount of rain, while the shift mode is energetically neutral. An extensive description of the methodology for calculating the rain amount and rain frequency distributions is presented in Pendergrass and Hartmann (2014b).

Here, we apply these two modes to the GCM response to CO_2 increase. In addition to the coherent modes of response, some models show an isolated response at heavy rain rates, which we call the extreme mode.

In the next section, we introduce the GCM dataset we will use. Then, we fit the modes of change to the rain amount response to CO_2 increase in these GCMs, consider the implications for the change in frequency distribution (particularly extreme events), and examine the differing responses across models.

2. Data and methods

In this section, we document the GCM simulations and observational datasets, and briefly describe our methodology. See the companion paper, Pendergrass and Hartmann (2014b), for a detailed description of how we calculate the distributions. We analyze daily rainfall accumulation from models and observations.

a. Daily rainfall data

To calculate the model precipitation distributions and their response to CO_2 doubling, we use climate model simulations from the CMIP5 archive (Taylor et al. 2012). We use simulations from two experiments: 1% yr^{-1} CO_2 increase (1pctCO2) and representative concentration pathway (RCP) with radiative forcing reaching 8.5 W m^{-2} in about 2100 (RCP8.5). The fully coupled 1pctCO2 scenario provides the response to CO_2 doubling, starting from a preindustrial control base state. We compare years 1–10 (the start of the simulation) and years 61–70 (CO_2 doubles at year 70). We use one ensemble member from each of the 22 models with archived daily rainfall accumulation and surface air temperature. The RCP8.5 experiment, which is also fully coupled, is a high emissions scenario, which also includes aerosol forcing and starts from historical simulations with greenhouse gas and aerosol forcing from 2005. From the RCP8.5 simulations, we compare 2006–15 with 2090–99. For models and scenarios where convective and large-scale precipitation are separately reported, we perform a separate analysis of these types of model precipitation.

For observational distributions of rainfall, we use a gridded observational dataset that merges data from satellite and rain gauges. Global Precipitation Climatology Project (GPCP) One-Degree Daily (1DD) data (Huffman et al. 2001) has global coverage at 1° resolution in latitude and longitude. We use data from 1997 to 2012.

b. Convective rain amount and rain frequency

Climate models calculate rain in two different ways: when a grid cell reaches saturation, they create large-scale (or resolved) precipitation, while a convective parameterization produces rain that represents events unresolved at the grid scale. We calculate two additional distributions using daily convective rainfall data. The first is the convective precipitation fraction in each bin of total rain rate. The second is the amount of convective precipitation falling in each total rain-rate bin. These are described in the appendix. We calculate rain amount and rain frequency distributions separately for the first 10 yr of the CO_2-doubling model simulations and the 10 yr immediately prior to doubling (years 61–70).

3. Modeled response to CO_2 doubling

a. The rain amount response

In this section we compare the response across CMIP5 models to CO_2 doubling using our modes of change as metrics. Water vapor increases at around 7% K^{-1}, and

previous work discussed in section 1 established that rate as a reasonable estimate of the change in extreme precipitation. What would the response of the rain distribution to a 7% increase or shift mode look like? Figure 1 shows the changes in terms of the rain amount, rain frequency, and the extreme precipitation response, along with the CMIP5 multimodel-mean response to CO_2 doubling. The shift and increase modes are introduced in the companion paper, Pendergrass and Hartmann (2014b).

To calculate the CMIP5 multimodel-mean response, the globally averaged rain amount and rain frequency distribution for each model are calculated for the first 10 yr of the simulation and for the 10 yr immediately prior to CO_2 doubling. The model distributions are averaged together to get the initial and doubled-CO_2 distributions. Finally, the initial rain amount and rain frequency distributions are subtracted from the doubled-CO_2 distributions, normalizing the change for each model by its increase in global-mean surface air temperature, to produce change estimates.

First, focus on the change in rain amount distribution in Figs. 1a,b. The CMIP5 multimodel-mean response has an increase at heavy rain rates and a decrease at moderate rain rates, though the total area under the change curve is positive (indicating increased total rainfall). The shift mode resembles the rain amount distribution change most closely, both in the amount of the change that it captures and in overall shape. Recall from section 1 that other studies have found an increase at high rain rates and decrease at moderate rain rates, reminiscent of this shift. The zero-crossing line of this shift occurs at the peak of the rain amount distribution, around 10 mm day^{-1}.

Now turn to the response in rain frequency distribution (Figs. 1c,d). The model response shows slight increases at heavy rain rates and decreases at moderate rain rates (consistent with the change in rain amount). It also has a slight increase at light rain rates, which play a negligible role in the rain amount distribution. Finally, dry-day frequency increases modestly. This pattern is consistent with Lau et al. (2013).

Both the increase and shift modes show some agreement with the change in frequency at high rain rates, but these make up only a small portion of the change in rain frequency (in contrast with rain amount). The model response has a small increase in dry-day frequency, consistent with the shift. Both the increase and shift of 7% K^{-1} drastically overestimate the comparatively modest changes in rain frequency.

Finally, focus on the extreme precipitation response (Figs. 1e,f). The model response is modestly negative below the 80th percentile, and increases with percentile steadily, reaching 7% K^{-1} at about the 99.99th percentile. The shift mode comes closest to matching the shape of the modeled extreme precipitation response, but it underestimates the response at the highest and lowest rain rates and overestimates it at moderate rain rates. In contrast, the increase mode has increases at all percentiles, which decrease with rain rate. It has dramatic increases in rain rate at moderate percentiles and more modest increases at the highest percentiles. If we were to add the increase and shift modes, the rain rate would increase by 7% at all percentiles. This would be consistent with the response at the 99.99th percentile, but it would overestimate the response in the rest of the distribution.

Instead of arbitrarily choosing the magnitude of the shift and increase modes, we can calculate the magnitudes that most closely fit the modeled response. The methodology for finding the optimal shift plus increase is described in Pendergrass and Hartmann (2014b).

The optimal shift plus increase for the multimodel-mean response is shown in Fig. 2. The magnitude of the shift mode is 3.3% K^{-1} and the increase mode is 0.9% K^{-1}. Between about 1 and 50 mm day^{-1}, the shift plus increase falls within the range of uncertainty in the model response. At the highest rain rates and at light rain rates, the shift plus increase underestimates the rain amount response. The error of the shift plus increase is 0.33 (33%), indicating that the shift plus increase captures all but a third of the modeled response.

The change in total rainfall captured by the shift plus increase is the same as the increase portion itself, 0.9% K^{-1}. The model response of total rainfall is 1.5% K^{-1}, which is larger. The missing rainfall occurs at heavy and light rain rates. Of the total error, 52% comes from the missing rain falling at rates of at least 40 mm day^{-1}, and 25% comes from the missing rain falling at rates below 2.5 mm day^{-1}.

We can also calculate the optimal shift plus increase for each model's response to CO_2 forcing. The responses for three models, along with their fitted shift plus increase, are shown in Fig. 3 (all models are shown in Fig. S1 of the supplemental material). Most but not all models share the increase in rain amount at high rain rates and decrease at lower rain rates. For some models, the shift plus increase fits the response quite closely, while for other models some aspects of the model response are captured but others are not (and, in two models, the shift plus increase does not resemble the model response at all).

We focus on just three models to illustrate the different types of extreme rain-rate response: Max Planck Institute Earth System Model, low resolution (MPI-ESM-LR; Giorgetta et al. 2013); L'Institut Pierre-Simon Laplace Coupled Model, version 5A, low

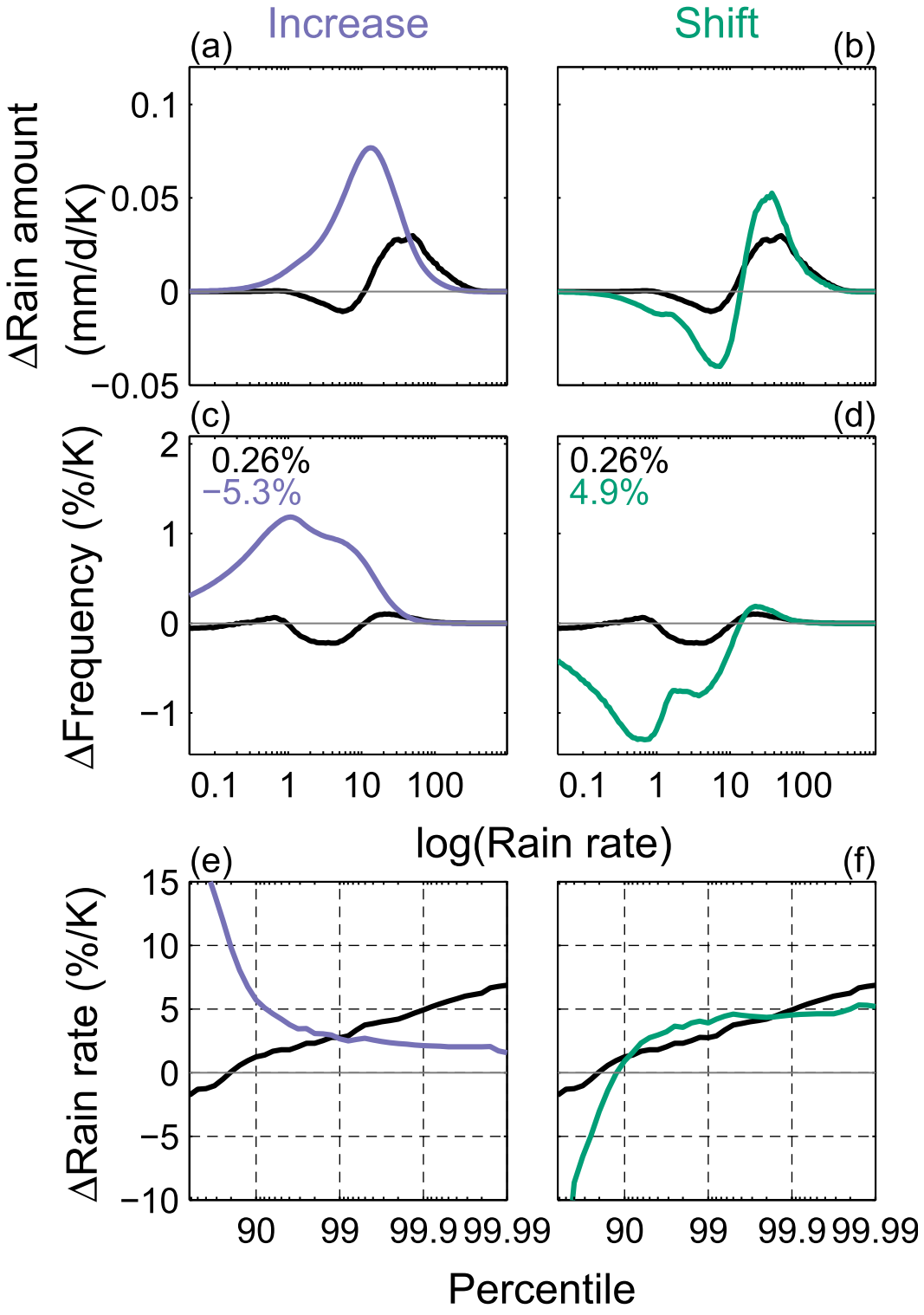

FIG. 1. The change in daily (a),(b) rain amount, (c),(d) rain frequency, and (e),(f) extreme rain in the CMIP5 multimodel-mean CO_2-doubling experiment (black) and the changes resulting from (left) an increase (purple) and (right) a shift (green) of the CMIP5 multimodel mean by 7%. The change in dry-day frequency of the CMIP5 multimodel mean (black) and each mode (color) is noted at the top left of (c),(d).

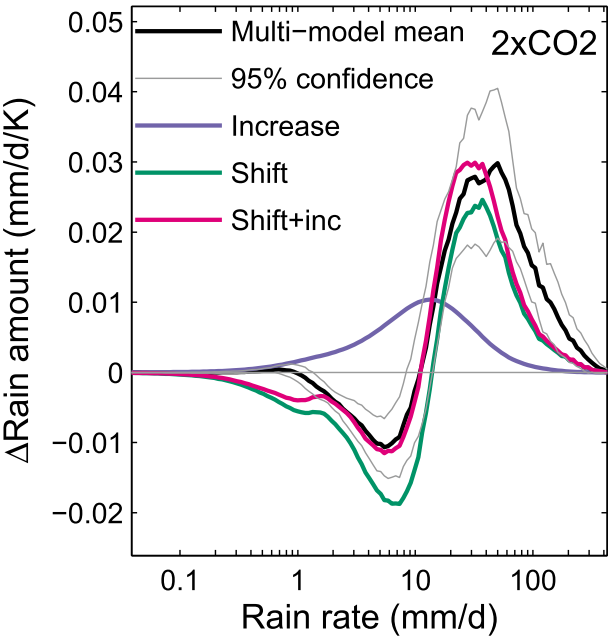

FIG. 2. CMIP5 multimodel-mean global rain amount response to CO_2 doubling (mm day^{-1} K^{-1}). The model response (black), increase (purple), shift (green), and shift plus increase (pink) are shown. Gray lines show 95% confidence interval of the multimodel-mean response.

resolution (IPSL-CM5A-LR; Dufresne et al. 2013); and Geophysical Fluid Dynamics Laboratory Earth System Model with Generalized Ocean Layer Dynamics component (GFDL-ESM2G; Dunne et al. 2012). We chose these models because they are clear examples, and most other models fall in between them. The model response that is best fit by the shift plus increase is MPI-ESM-LR (Fig. 3a). This model also has one of the two largest shifts. The shift-plus-increase fit to the MPI-ESM-LR precipitation change captures both the decrease in rain amount at moderate rain rates and the increase at the heaviest rates. In contrast, the shift plus increase fits the IPSL-CM5A-LR (Fig. 3b) and GFDL-ESM2G (Fig. 3c) models less closely. The modeled responses and shift plus increase for both models have a resemblance, especially at the primary peak at high rain rates and dip at moderate rain rates. However, the shift plus increase does not capture an additional increase at the heaviest rain rates in either model. Models with larger shifts have smaller error (Fig. 4). Across all models, the increase mode ranges from 0.3% to 2.4% K^{-1}. The shift mode ranges from 5.8% to −0.16% K^{-1}. Errors of the fit range from 14% to 93%. The averages of the model responses, along with the multimodel mean, are listed in Table 1.

Instead of fitting the increase, we can simply use the percentage change in total rainfall as the increase. This forces the entire increase in rainfall to occur evenly across the distribution. Then, we can do a one-parameter fit of only the shift. This makes no qualitative difference on the magnitude of the shift, but increases the error of the multimodel-mean fit and most of the model fits.

For all but two models, the fitted increase is smaller than the model's total rainfall change (Fig. 4). One explanation is that only some of the change in total rainfall is captured by a uniform increase of the mean distribution.

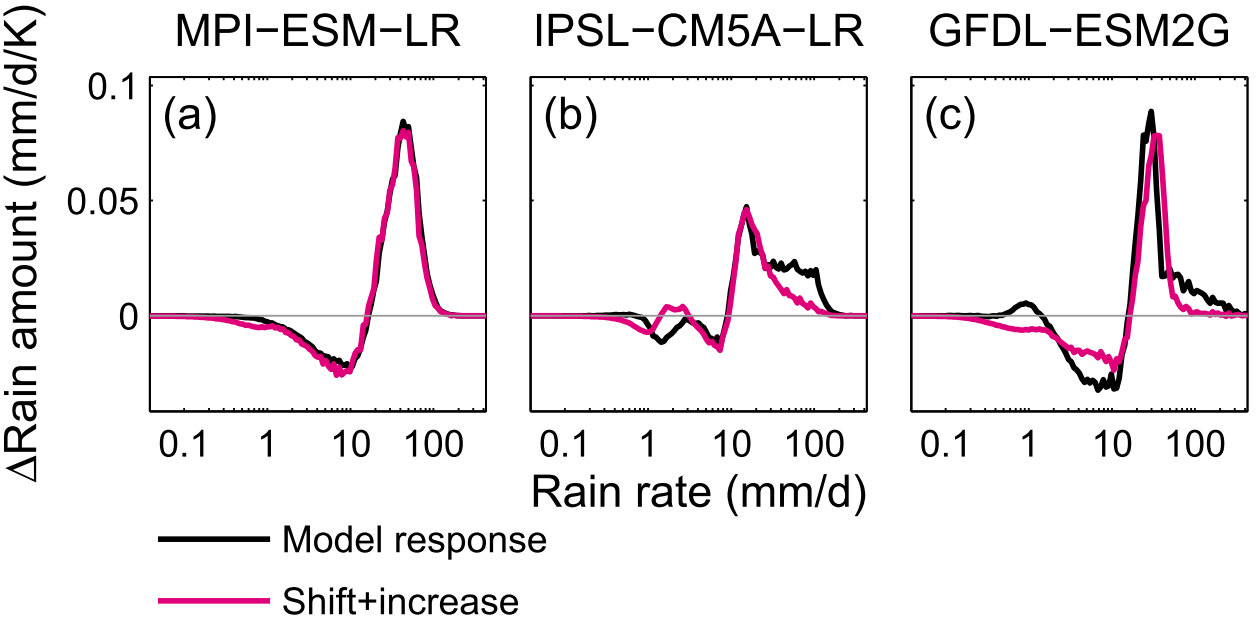

FIG. 3. Rain amount response to CO_2 doubling (black) for three of the CMIP5 models and their fitted shift plus increase (pink).

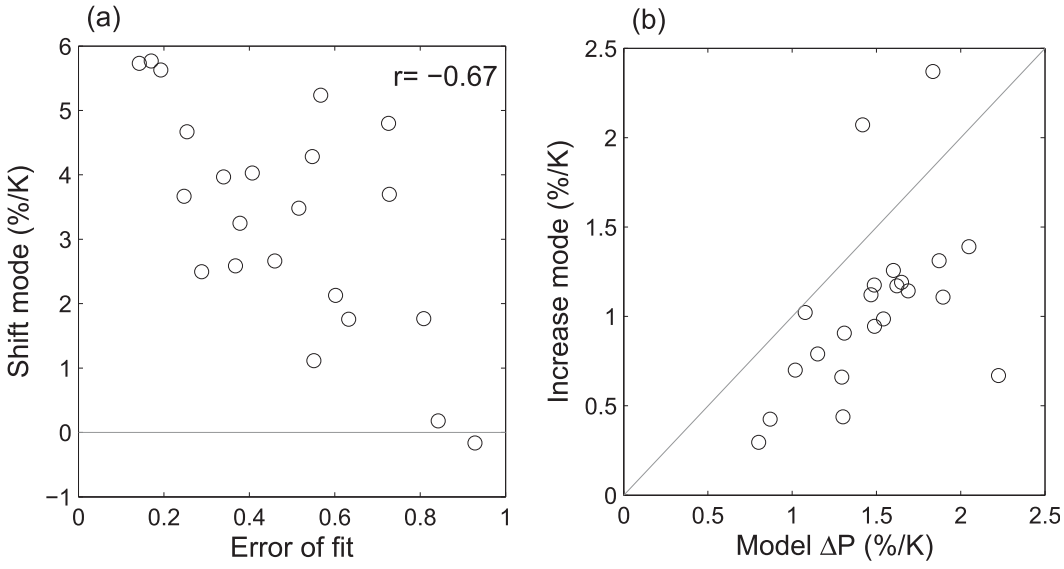

FIG. 4. (a) Magnitude of shift mode (% K^{-1}) vs error of the fit (unitless fraction). The correlation is at the top right. (b) Global-mean precipitation increase vs magnitude of the increase mode for each model (% K^{-1}). The gray line in (b) shows the 1:1 relationship.

The rest occurs as a change isolated at light or heavy rain rates, and unrelated to the changes across the rest of the distribution. We will return to this missing rainfall below.

Tropical and extratropical precipitation distributions could respond differently. Studies of extreme precipitation find that extratropical precipitation change is more readily decomposed into thermodynamic and dynamic components than tropical precipitation (e.g., O'Gorman and Schneider 2009). Table 1 shows fits of both shift and increase parameters to the tropical and extratropical regions in each model (split at 30°). The fit has lower error in the extratropics than the tropics. The extratropics generally have a bigger increase (1.3% K^{-1}) and bigger shift (4.0% K^{-1}), while the tropics have a smaller increase (0.6% K^{-1}) and shift (2.9% K^{-1}). Unlike the differences between tropics and extratropics, the differences between land and sea are modest. The land has a slightly larger shift (3.5% K^{-1}) than sea (3.1% K^{-1}), while both have an increase of 0.9% K^{-1}. This is in sharp contrast to precipitation changes during El Niño events, for which changes over land and ocean are very different (Pendergrass and Hartmann 2014b).

So far we have shown that in the multimodel mean for CMIP5 models forced by CO_2 doubling, the distribution of rain amount shifts to higher rain rates by 3.3% K^{-1} and increases by 0.9% K^{-1}. This reasonably fits the change in much of the distribution of rain amount. Next, we will discuss how the increase and shift modes fit the rain frequency response.

b. *Implications for the frequency distribution*

Figure 5 shows the change in rain frequency in the CMIP5 multimodel mean, along with the fitted shift and increase modes and the shift plus increase. In the model response, the decrease in rain frequency is largest at moderate rain

TABLE 1. The shift and increase in response to CO_2 doubling in CMIP5 model simulations, along with the error of the fit. Fit to the multimodel-mean response is on the left and average of the fits to each model's response is on the right. Shifts, increases, and ΔP have units of percent per kelvin, where changes are normalized by the global-mean surface air temperature change. The error is the absolute value of the difference in rain amount normalized by the target change in rain amount.

Region	Change in model mean			Mean of model changes			Actual
	Shift (% K^{-1})	Increase (% K^{-1})	Error	Shift (% K^{-1})	Increase (% K^{-1})	Error	ΔP (% K^{-1})
Global	3.3	0.94	0.33	3.3	1.1	0.49	1.5
Sea	3.1	0.94	0.36	3.1	1.0	0.52	1.4
Land	3.5	0.86	0.49	3.7	0.99	0.53	1.8
Extratropics	4.0	1.3	0.34	3.9	1.3	0.36	1.9
Tropics	2.9	0.56	0.43	3.1	0.78	0.50	1.2

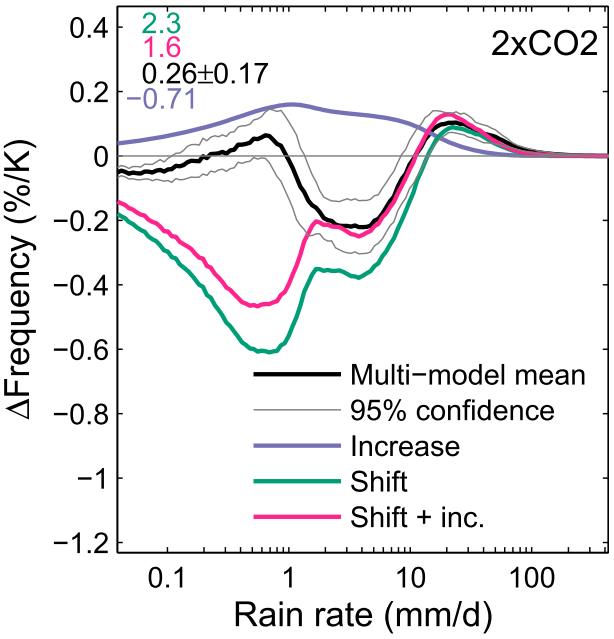

FIG. 5. Rain frequency response to CO_2 doubling in CMIP5 models (% K^{-1}), with change in dry-day frequency noted at the top left. The multimodel-mean response (black), increase (purple), shift (green), and shift plus increase (pink) are shown.

rates. The multimodel-mean change in dry-day frequency in models is 0.26% ± 0.17% K^{-1}.

The fitted shift plus increase is not as close as it is for rain amount. The shift mode has the largest decreases in frequency at light rain rates around 1 mm day^{-1}. But instead of a large decrease in the frequency of light rain, the models have an increase, which occurs entirely over ocean (Pendergrass 2013). This light rain mode accounts for some of the total rainfall increase that is not present in the shift plus increase. But, as is discussed in Pendergrass and Hartmann (2014b), light rain makes up only a small fraction of the total rainfall, and models have much more frequent light rain than observations. The shift plus increase has a 1.6% K^{-1} increase in dry-day frequency. The difference in dry-day frequency response between models and the shift plus increase is probably related in part to the increase in frequency of light rain. Because the integral over the frequency distribution must sum to one, differences in frequency response at one rain rate must be balanced by differences of the opposite sign at another rain rate. The larger increase in dry-day frequency of the shift plus increase compared to the model response is balanced by the large decrease at light rain rates (which is due to the light rain mode).

c. *Extreme events*

Now, we take a closer look at changes in extreme precipitation. Figure 6 shows the percent change in rain rate as a function of percentile of the cumulative frequency distribution for the multimodel-mean response to increased CO_2. As in Allen and Ingram (2002) and Pall et al. (2007), we find a decrease in rain rate below the 90th percentile and increase above the 90th percentile in the multimodel-mean response to CO_2 doubling. The percentage increase in rain rate goes up with the percentile. At the 99.9th percentile, the increase is 4.9% K^{-1}, consistent with O'Gorman and Schneider (2009), though they looked at zonal-mean changes in CMIP3 models. At the 99.99th percentile, the increase in rain rate is 6.9% K^{-1}.

The shift plus increase, which was fit to the rain amount distribution, has some similarities to and also some differences from the modeled response. The shift plus increase is the sum of the increase and shift modes (the shapes of which are shown in Figs. 1e,f). Below the 90th percentile, the shift plus increase crosses from negative to positive. These negative changes indicate a decrease in the rate of light rain events, which is due to the shift. Between the 90th and 99th percentiles, the shift plus increase flattens with continued increase in percentile. All events beyond the 99th percentile increase between 3% and 4% K^{-1}, in contrast to the continued increase with percentile of the model response. The shape of this part of the shift plus increase depends on the relative magnitude of the shift and increase modes as well as the shape of the initial rain frequency distribution.

The right panels of Fig. 7 show three models' change in rain rate as a function of percentile along with their fitted shift plus increase for the RCP8.5 experiment (all models are shown for the CO_2-increase experiment in Fig. S2 of the supplemental material; we use RPC8.5 here because more models archive convective precipitation for RCP8.5 than for the CO_2-increase experiment). There are two types of model responses: those that increase by a similar percentage for all extreme precipitation (beyond the 99th percentile) and those that increase most at the most extreme percentiles. The responses with similar increases for all extreme percentiles are well captured by the shift plus increase. In contrast, responses that increase most at the most extreme percentiles are not captured. We will call this uncaptured response the extreme mode. Other studies have also shown the model responses fall into two camps. Sugiyama et al. (2010) found that extreme precipitation increased by more than water vapor in half of CMIP3 model simulations.

The tropics have a slightly larger increase in rain rate at the 99.99th percentile, 8.7% K^{-1}, than the extratropics, 6.5% K^{-1}. However, models agree much more closely on the extratropical response than on the tropical response (Figs. S3, S4 in the supplemental material). In the tropics, the standard deviation of the 99.99th-percentile rain-rate response across models is 6.3% K^{-1}, while in the extratropics it is just 1.7% K^{-1}. Previously, O'Gorman and Schneider (2009) found that extratropical

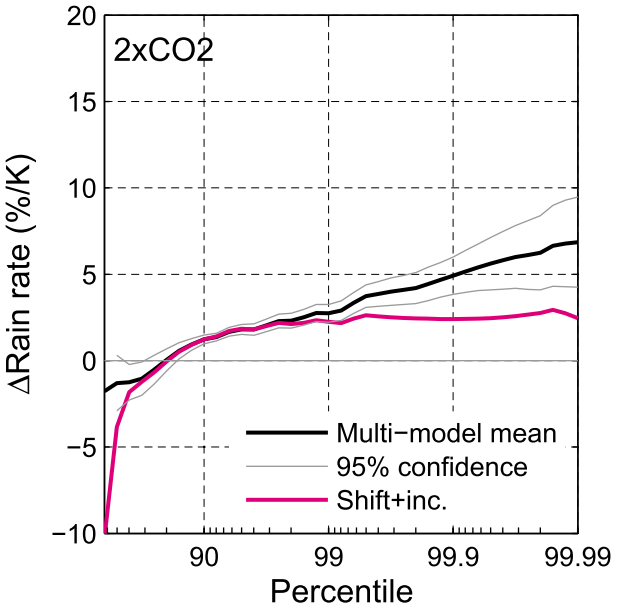

FIG. 6. Extreme precipitation response ($\%\,K^{-1}$) for CMIP5 multimodel-mean CO_2 doubling (black) and the shift plus increase (pink): percent change in rain rate per kelvin warming as a function of the percentile of the cumulative frequency distribution. Gray lines show 95% confidence of the multimodel-mean response.

extreme precipitation change follows the moisture convergence scaling law more closely than tropical change. In Table 1, we saw that, in the extratropics, the shift mode was bigger and the error of the shift plus increase was smaller than in the tropics. The difference in shift mode, error, and extreme rain are consistent with a bigger extreme mode response in the tropics than in the extratropics. We will consider the differences across models next.

d. *Differences across models: Resolved and unresolved rain events*

Why does the extreme rain-rate response to CO_2 doubling follow the shift plus increase so closely in some models, but increase much more in other models? In this section, we focus on a subset of models to explore the extreme mode behavior in more detail.

Convective parameterizations are an important difference between models, and they are important for modeled rainfall. Climate models form rain in two ways. When the grid-scale environment is saturated, the model produces large-scale precipitation. Whether or not a grid box is saturated, the convective parameterization produces precipitation, which represents the rain coming from unresolved motions.

Neither large-scale nor convective precipitation is obviously more realistic than the other. As model resolution increases, more motions are resolved, so more precipitation should be large-scale and less should be convective. Increasing model resolution decreased the bias in extreme precipitation over land compared to observations (Kopparla et al. 2013). Large-scale and convective precipitation are not independent. When convective precipitation is inhibited, large-scale precipitation increases to compensate (Lin et al. 2013). Large-scale and convective precipitation do not correspond to the classification of observed stratiform and convective precipitation types (Held et al. 2007). Mesoscale organization relevant to realistic heavy precipitation is not represented in climate models (Rossow et al. 2013). While large-scale and convective events are comparably realistic (or unrealistic), this division of precipitation is an artifact of modeling, rather than a realistic description of two types of precipitating systems.

Heavy, predominantly large-scale rain events are found in models, and the extent to which they are realistic is unclear. Held et al. (2007) called these events gridpoint storms. They showed, with idealized simulations of a model related to the GFDL-ESM atmospheric model, that gridpoint storms appear above a threshold temperature, and with further warming the amount of rain from gridpoint storms increases. The threshold temperature, but not the overall behavior, depends on resolution.

We would like to investigate how resolved (large scale) and unresolved (convective) precipitation play a role in the model-dependent extreme precipitation response we see. Daily convective precipitation data are available for just eight of the models in the CO_2-doubling experiment. Unfortunately, all of the models with available daily convective precipitation data for this experiment have increases in extreme rain rate that are much greater than the prediction from the shift plus increase, so that the models without this feature are not available with daily convective precipitation data. More modeling groups archive both total and convective precipitation at daily time scales for the realistic-forcing RCP8.5 scenario than for the CO_2-increase scenario. In the models we examine here, the rain amount distribution response is similar between the RCP8.5 and CO_2-increase experiments, so we will investigate the RCP8.5 simulations.

Figure 7 shows key aspects of the three models' rain amount distributions and responses to realistic forcing in the RCP8.5 experiment: the rain amount distribution compared to coarsened GPCP, the climatological convective fraction as a function of cumulative frequency distribution, the rain amount response to warming (total change simulated by the models, convective precipitation contribution to the total, and the fit by the shift plus increase), and the extreme precipitation response.

The MPI-ESM-LR rain amount response to warming is captured most closely of all the models by the shift plus increase (Fig. S1 in the supplemental material). Its change in rain amount looks like the ideal shift and increase illustrated partially in Fig. 1. It has one of the

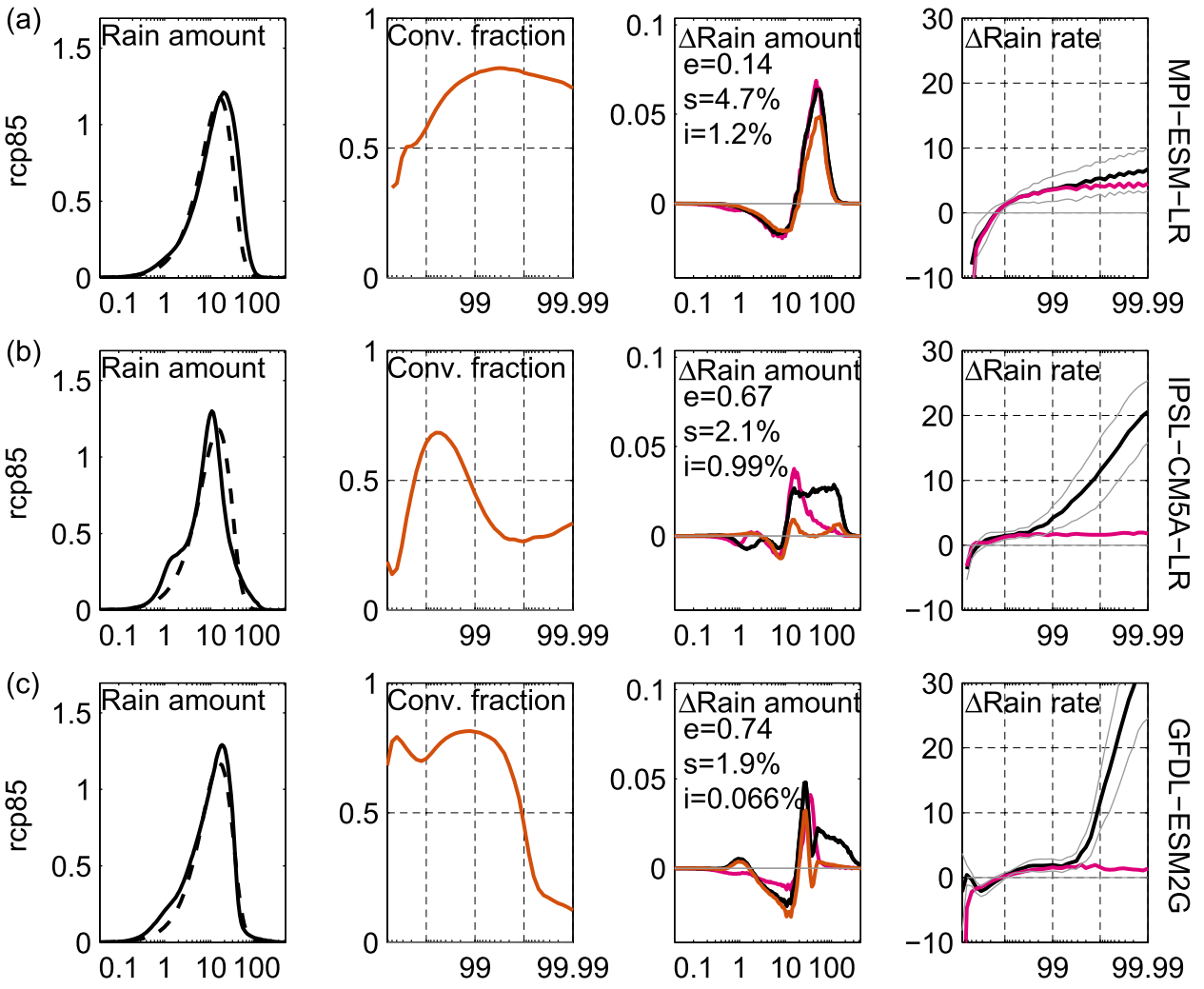

FIG. 7. Global (a) MPI-ESM-LR, (b) IPSL-CM5A-LR, and (c) GFDL-ESM2G model responses in the RCP8.5 scenario. (left) The rain amount climatology, the *i*th model distribution (solid black) shown along with coarsened GPCP (dashed). (left center) The climatological convective fraction, shown alone (orange). (right center) The change in rain amount distribution, with the model change (black), shift plus increase (pink), and convective precipitation change (orange) shown. The error *e*, shift *s*, and increase *i* magnitudes are included. (right) The change in extreme rain rate, with the model change (black) and shift plus increase (pink) shown.

largest shifts of any model in the CO_2-increase experiment, 5.7% K^{-1} (only MPI-ESM-P is higher at 5.8% K^{-1}; Fig. S1). For the CO_2-doubling simulation, its extreme precipitation response is captured very well by the shift plus increase. Its extreme precipitation response in RCP8.5 is captured almost as closely. Furthermore, the shape of the rain amount distribution of MPI-ESM-LR matches the coarsened GPCP rain amount distribution very closely compared to most other models.

IPSL-CM5A-LR and GFDL-ESM2G contrast with the MPI response. The shift plus increase only partially captures their response to warming, with errors of 67% and 74% (Fig. 7). In both models, the shift plus increase captures a dip in rain amount at moderate rain rates and the increase at rain rates just above this. However, it fails to capture increases in rain amount at the highest rain rates in these two models. In both cases, these additional increases in rain amount look like extra rain has been added to the high side of the distribution (in contrast to the MPI-ESM-LR response). The extreme rain-rate response also differs from the shift plus increase in these models. GFDL-ESM2G has the largest 99.99th-percentile rain-rate increase of any model, and the IPSL-CM5A-LR response is among the largest. The shift fit to both of these responses is lower than it is for many models, around 2% K^{-1} (it is greater for both models in the CO_2-doubling experiments; Fig. S1), but their increases in extreme rainfall are much greater even than models with large shifts.

How much of the rain amount response is convective rainfall, and how much is large scale? Measures of

convective rainfall were described in section 2 and are shown in the appendix. The change in the amount of convective precipitation in each rain-rate bin is shown in orange in Fig. 7. In MPI-ESM-LR, the majority of the change in rain amount is convective. There is just a small difference between convective and total precipitation near the peak of the increase, which is an increase in large-scale precipitation. In contrast, the IPSL-CM5A-LR change in convective rain amount is very small, indicating that most of the change in rain amount is large-scale precipitation. While some of this increase is captured by the shift plus increase, much of it is not. The increases at the highest rain rates, which are not captured by the shift plus increase, are changes in large-scale precipitation. In GFDL-ESM2G, there are two peaks at the high end of the rain amount response. The highest peak, at moderate rain rates near 10 mm day^{-1}, is mostly convective rainfall and is captured by the shift plus increase. The smaller peak, which is at higher rain rates, is mostly large-scale precipitation and is not captured by the shift plus increase. As in the case of the IPSL-CM5A-LR model, this uncaptured large-scale increase in rain amount accounts for the large increase in rain rate at the highest cumulative probabilities.

Held et al. (2007) suggested that the sensitivity of gridpoint storms in any particular model might be related to the fraction of convective precipitation in the model. Motivated by this, we calculate the climatological fraction of convective precipitation as a function of cumulative probability distribution in each of the models. In MPI-ESM-LR, rainfall at the 99.99th percentile at the beginning of the twenty-first century is about 75% convective and only 25% large scale. In IPSL-CM5A-LR, about 30% of 99.99th-percentile precipitation is convective, with more large-scale than convective precipitation above the 99th percentile. In GFDL-ESM2G, less than 20% of the 99.99th-percentile rainfall is convective and large-scale precipitation makes up 80% of the rainfall above the 99.9th percentile. The divergence of the extreme rain-rate response from the shift-plus-increase fit in these models occurs around the percentile where large-scale rain fall begins to constitute a majority. The driver of the differences in extreme rain-rate response across models is the fraction of the events that occur as large-scale precipitation in the climatological distribution, suggesting a strong role for gridpoint storms in producing these extremes.

When the analysis is repeated for the extratropics alone (Fig. S3 in the supplemental material), model responses deviate much less from the shift plus increase than in the global distribution. In most models, there is a small increase in the model response beyond the multimodel mean, but this difference is similar in all models and much more modest than the extreme mode seen globally. In contrast, when the analysis is restricted to the tropics (Fig. S4), the variations across models in the extreme mode are dramatic. Taken together, these additional analyses indicate that the extreme mode occurs mainly in the tropics, rather than in the extratropics.

Gridpoint storms as a driver of extreme precipitation in some but not all models may provide an explanation for the nonlinear response of the tropical extreme precipitation (in terms of changing vertical velocity and moisture gradient) found in previous studies. The model whose 99.9th-percentile rain response was least captured by the precipitation extremes scaling in O'Gorman and Schneider (2009) was GFDL Climate Model, version 2.0 (CM2.0); the atmospheric model in GFDL-ESM2G is similar to CM2.1 (Dunne et al. 2012). This scaling assumes that changes in precipitation are linearly related to changes in moisture and vertical velocity, whereas gridpoint storms may not respond in this fashion.

4. Discussion

a. *Summary of changes in the distribution of rain*

With the analysis above, we are in a position to describe three components of the rain amount response to CO_2 doubling. First, the rain amount distribution shifts to higher rain rates, and this is captured by the shift plus increase. For CO_2 doubling, the shift of 3.3% K^{-1} in the multimodel mean indicates that the same amount of rain falls at 3.3% K^{-1} higher rain rates, with fewer total events. Simultaneously, the rain frequency and amount distributions increase by 0.9% K^{-1}. The error of this fit is 0.3, and the increase accounts for 0.9 of 1.5% K^{-1}; both of which indicate that the shift plus increase describes about two-thirds of the change in rain distribution in response to CO_2 doubling.

The rest of the increase in rain amount comes as deviations from this coherent response. A small contribution comes as an increase in light rain over ocean, unrelated to changes in the distribution. Observations disagree with models on the climatological frequency of light rain. Both models and observations contain uncertainty, so it is not clear whether modeled light rain and its response are realistic.

The final contribution to the rainfall increase that is not captured by the shift plus increase is an increase at the highest rain rates occurring in some but not all models, which we have argued is due to an increase in gridpoint storms. (Two examples of the evolution of a 99.99th-percentile event are shown in Figs. S6 and S7 of the supplemental material.) These gridpoint storms contribute most of the remaining third of the increase in total rainfall in the multimodel mean in response to CO_2 doubling.

Furthermore, as warming increases, more of the precipitation increase comes as an increase in gridpoint storms and less comes as a coherent shift and increase of the rain amount distribution (Table S1 and Fig. S8 in the supplemental material). Gridpoint storms are likely model artifacts. The large sensitivity of extreme rain response shown here demonstrates the need for improved representation of extreme rain events in climate models.

b. Reconciling energetic and moisture constraints

We are also in a position to articulate how energetic and moisture constraints can be simultaneously met. First, the energetic constraint is met by the total increase in rain amount. Above, we saw that this consists primarily of the increase mode, and secondarily the extreme mode.

However, moisture and moisture convergence increase much more than the total rainfall. How can the apparent discrepancy between the large increase in moisture and the smaller increase in rain rate be accounted for? Our analysis suggests two possibilities. First, consider models like MPI-ESM-LR with no extreme mode, in which the extreme precipitation change follows closely the shift plus increase. The increase mode results in a change in rain rate of just 1.3% K^{-1} for the heaviest events, not enough to account for the increased moisture convergence. To make up the difference, the energetically neutral shift mode provides a mechanism for further increases in the heaviest rain rates. The same amount of rain falls at heavier rain rates, so that increased moisture convergence can be accommodated without violating the energetic constraint or requiring further increases in atmospheric radiative cooling. In this scenario, there would be fewer events governed by moisture convergence, because the shift mode decreases the frequency of rain events, implying an increase in dry-day frequency (the MPI models have the biggest increase in dry-day frequency).

On the other hand, consider models with an extreme mode, like the IPSL and GFDL models. In these models, the extreme rain-rate response and the moisture constraint are met by the extreme mode instead of the shift mode. These large increases of extreme rain rate are not accompanied by changes in the rest of the distribution, such as increases in dry-day frequency, since they contribute little to the total frequency.

5. Conclusions

We have considered the change in rain amount and rain frequency distribution of daily precipitation data in response to CO_2 increase in CMIP5 models. In the shift mode of the distribution of rain, the same amount of rain falls at rain rates a fixed percentage higher. In the increase mode, a fixed percentage more rain falls at every rain rate. We fit the shift and increase modes of the rain amount distribution to the modeled response to CO_2 increase and considered the coherent response as well as the deviations from it. In response to CO_2 doubling in CMIP5 models, the rain amount distribution shifts by 3.3% K^{-1} and increases by about 1% K^{-1}.

In response to CO_2 doubling, some of the models have increases of extreme precipitation (greater than the 99th percentile) that closely follow the shift plus increase fitted to each model's change in rain amount distribution. Other models produce much bigger increases in extreme precipitation than the shift plus increase, which we call the extreme mode, indicating that extreme precipitation change is not tied to the change in the rest of the rain amount distribution in these models. We attribute these additional increases in very heavy rain rate to changes in large-scale precipitation probably related to gridpoint storms.

These results indicate that with warming, rainfall shifts to higher rain rates, as argued by Trenberth (1999), but the rate of change is smaller than the increase in moisture and extreme events. The very high rate of increase of extreme precipitation found in some studies (e.g., Allen and Ingram 2002; Sugiyama et al. 2010; O'Gorman 2012) is not associated with changes in the rest of the distribution of rain.

Acknowledgments. CMIP5 modeling groups generously shared their simulations, and the resulting data were distributed by PCMDI. GPCP also generously made their data available. This work was funded by NSF under Grant AGS-0960497. We thank Dargan Frierson for encouraging discussions and three anonymous reviewers and Anthony Broccoli for feedback that improved the manuscript.

APPENDIX

Convective Rain Amount and Rain Frequency Distribution Calculations

We use the daily convective rainfall accumulation r_{conv} to calculate the distribution of convective rain amount p^{conv} and convective precipitation fraction f^{conv} in each bin of total daily rain accumulation r,

$$p_i^{\text{conv}}(R_i^c) = \frac{1}{\Delta \ln R} \sum_{\text{gridpts}} r_{\text{conv}}(R_i^l \le r \le R_i^r) \frac{A_{\text{gridpt}}}{A_{\text{total}}} \quad \text{and} \tag{A1}$$

$$f_i^{\mathrm{conv}}(R_i^c) = \frac{1}{\Delta \ln R} \sum_{\mathrm{gridpts}} \frac{r_{\mathrm{conv}}}{r}(R_i^l \le r \le R_i^r) \frac{A_{\mathrm{gridpt}}}{A_{\mathrm{total}}}, \tag{A2}$$

where R_i^l and R_i^r are left and right bin edges, $R_i^c = (R_i^l + R_i^r)/2$ is bin centers, and A indicates the area of each grid point and the total area.

REFERENCES

Allan, R. P., B. J. Soden, V. O. John, W. Ingram, and P. Good, 2010: Current changes in tropical precipitation. *Environ. Res. Lett.,* **5,** 025205, doi:10.1088/1748-9326/5/2/025205.

Allen, M. R., and W. J. Ingram, 2002: Constraints on future changes in climate and the hydrologic cycle. *Nature,* **419,** 224–232, doi:10.1038/nature01092.

Chou, C., C.-A. Chen, P.-H. Tan, and K. T. Chen, 2012: Mechanisms for global warming impacts on precipitation frequency and intensity. *J. Climate,* **25,** 3291–3306, doi:10.1175/JCLI-D-11-00239.1.

Dufresne, J.-L., and Coauthors, 2013: Climate change projections using the IPSL-CM5 Earth system model: From CMIP3 to CMIP5. *Climate Dyn.,* **40,** 2123–2165, doi:10.1007/s00382-012-1636-1.

Dunne, J. P., and Coauthors, 2012: GFDL's ESM2 global coupled climate–carbon Earth system models. Part I: Physical formulation and baseline simulation characteristics. *J. Climate,* **25,** 6646–6665, doi:10.1175/JCLI-D-11-00560.1.

Emori, S., and S. Brown, 2005: Dynamic and thermodynamic changes in mean and extreme precipitation under changed climate. *Geophys. Res. Lett.,* **32,** L17706, doi:10.1029/2005GL023272.

Giorgetta, M. A., and Coauthors, 2013: Climate and carbon cycle changes from 1850 to 2100 in MPI-ESM simulations for the Coupled Model Intercomparison Project phase 5. *J. Adv. Model. Earth Syst.,* **5,** 572–597, doi:10.1002/jame.20038.

Held, I. M., and B. J. Soden, 2006: Robust responses of the hydrological cycle to global warming. *J. Climate,* **19,** 5686–5699, doi:10.1175/JCLI3990.1.

——, M. Zhao, and B. Wyman, 2007: Dynamic radiative–convective equilibria using GCM column physics. *J. Atmos. Sci.,* **64,** 228–238, doi:10.1175/JAS3825.11.

Huffman, G. J., R. F. Adler, M. M. Morrissey, D. T. Bolvin, S. Curtis, R. Joyce, B. McGavock, and J. Susskind, 2001: Global precipitation at one-degree daily resolution from multisatellite observations. *J. Hydrometeor.,* **2,** 36–50, doi:10.1175/1525-7541(2001)002<0036:GPAODD>2.0.CO;2.

Kopparla, P., E. Fischer, C. Hannay, and R. Knutti, 2013: Improved simulation of extreme precipitation in a high resolution atmosphere model. *Geophys. Res. Lett.,* **40,** 5803–5808, doi:10.1002/2013GL057866.

Lau, W. K.-M., H.-T. Wu, and K.-M. Kim, 2013: A canonical response of precipitation characteristics to global warming from CMIP5 models. *Geophys. Res. Lett.,* **40,** 3163–3169, doi:10.1002/grl.50420.

Lin, Y., M. Zhao, Y. Ming, J.-C. Golaz, L. J. Donner, S. A. Klein, V. Ramaswamy, and S. Xie, 2013: Precipitation partitioning, tropical clouds, and intraseasonal variability in GFDL AM2. *J. Climate,* **26,** 5453–5466, doi:10.1175/JCLI-D-12-00442.1.

Mitchell, J. F. B., C. A. Wilson, and W. M. Cunnington, 1987: On CO_2 climate sensitivity and model dependence of results. *Quart. J. Roy. Meteor. Soc.,* **113,** 293–322, doi:10.1256/smsqj.47516.

O'Gorman, P. A., 2012: Sensitivity of tropical precipitation extremes to climate change. *Nat. Geosci.,* **5,** 697–700, doi:10.1038/ngeo1568.

——, and T. Schneider, 2009: The physical basis for increases in precipitation extremes in simulations of 21st-century climate change. *Proc. Natl. Acad. Sci. USA,* **106,** 14 773–14 777, doi:10.1073/pnas.0907610106.

Pall, P., M. Allen, and D. Stone, 2007: Testing the Clausius–Clapeyron constraint on changes in extreme precipitation under CO_2 warming. *Climate Dyn.,* **28,** 351–363, doi:10.1007/s00382-006-0180-2.

Pendergrass, A., 2013: The atmospheric energy constraint on precipitation change. Ph.D. dissertation, University of Washington, 134 pp.

——, and D. L. Hartmann, 2014a: The atmospheric energy constraint on global-mean precipitation change. *J. Climate,* **27,** 757–768, doi:10.1175/JCLI-D-13-00163.1.

——, and ——, 2014b: Two modes of change of the distribution of rain. *J. Climate,* **27,** 8357–8371, doi:10.1175/JCLI-D-14-00182.1.

Rossow, W. B., A. Mekonnen, C. Pearl, and W. Goncalves, 2013: Tropical precipitation extremes. *J. Climate,* **26,** 1457–1466, doi:10.1175/JCLI-D-11-00725.1.

Stephens, G. L., and T. D. Ellis, 2008: Controls of global-mean precipitation increases in global warming GCM experiments. *J. Climate,* **21,** 6141–6155, doi:10.1175/2008JCLI2144.1.

Sugiyama, M., H. Shiogama, and S. Emori, 2010: Precipitation extreme changes exceeding moisture content increases in MIROC and IPCC climate models. *Proc. Natl. Acad. Sci. USA,* **107,** 571–575, doi:10.1073/pnas.0903186107.

Sun, Y., S. Solomon, A. Dai, and R. W. Portmann, 2007: How often will it rain? *J. Climate,* **20,** 4801–4818, doi:10.1175/JCLI4263.1.

Taylor, K. E., R. J. Stouffer, and G. A. Meehl, 2012: An overview of CMIP5 and the experiment design. *Bull. Amer. Meteor. Soc.,* **93,** 485–498, doi:10.1175/BAMS-D-11-00094.1.

Trenberth, K. E., 1999: Conceptual framework for changes of extremes of the hydrological cycle with climate change. *Climatic Change,* **42,** 327–339, doi:10.1023/A:1005488920935.

——, 2011: Changes in precipitation with climate change. *Climate Res.,* **47,** 123–138, doi:10.3354/cr00953.

Supplement to: Changes in the distribution of rain frequency and intensity in response to global warming

Angeline G. Pendergrass[1] and Dennis L. Hartmann
Department of Atmospheric Sciences, University of Washington, Seattle

[1] Corresponding author address: Angeline G. Pendergrass, NCAR, P.O. Box 3000, Boulder, CO 80307.
E-mail: apgrass@ncar.edu

List of Tables

Table S1: Mean of model responses to CO_2 doubling, tripling, and quadrupling. The units for most variables are % K^{-1}. Exceptions are the global-mean temperature increase ΔT, which has units of K, and the error, which is a unitless fraction.

TABLE S1. Mean of model responses to CO_2 doubling, tripling, and quadrupling. The units for most variables are % K^{-1}. Exceptions are the global-mean temperature increase ΔT, which has units of K, and the error, which is a unitless fraction.

	Fit		Actual	$\Delta R_{99.99}$			
CO_2	Shift	Inc.	ΔP	Fit	Actual	Error	ΔT
	(% K^{-1})		(% K^{-1})	(% K^{-1})			(K)
2x	3.3	1.1	1.5	2.9	8.4	0.49	1.7
3x	3.2	0.94	1.5	2.8	10	0.53	3.0
4x	3.0	0.92	1.5	2.6	12	0.54	4.1

List of Figures

Figure S1: Rain amount response to CO_2 doubling for each CMIP5 model and its shift, increase, and shift-plus-increase fit. At top left error (*e*), shift (*s*) and increase (*i*) are listed. Models are ordered from smallest to largest error.

Figure S2: Extreme precipitation response (% K^{-1}) to CO_2 doubling in each CMIP5 model (black) and its shift-plus-increase (magenta).

Figure S3: Extra-tropical extreme precipitation response (% K^{-1}) to CO_2 doubling in each CMIP5 model (black) and its shift-plus-increase (magenta).

Figure S4: Tropical extreme precipitation response (% K^{-1}) to CO_2 doubling in each CMIP5 model (black) and its shift-plus-increase (magenta).

Figure S5: Maps of the rain amount (mm d^{-1}) falling in the top 0.1% of events from the first ten years of the RCP8.5 scenario in MPI-ESM-LR (top left) and GFDL-ESM2G (bottom left) model simulations and GPCP (top right) and TRMM 3B42 (bottom right) observations. Boxes for each model show the subdomain in Figures S6 and S7.

Figure S6: Rain rate and convective rain (mm d^{-1}) for a 99.99th percentile event in the MPI-ESM-LR model chosen from the first ten years of the RCP8.5 simulation.

Figure S7: Rain rate and convective rain (mm d^{-1}) for a 99.99th percentile event in the GFDL-ESGM2G model chosen from the first ten years of the RCP8.5 simulation.

Figure S8: MPI-ESM-LR (top left), IPSL-CM5A-LR (top right), and GFDL-ESM2G (bottom) models 2x (top) and 4xCO_2 (bottom) rain amount (left) and extreme rain rate (right) responses. Model response (black) and shift-plus-increase (magenta). Error *e*, shift *s*, and increase *i* are noted in the top left of the rain amount response panels.

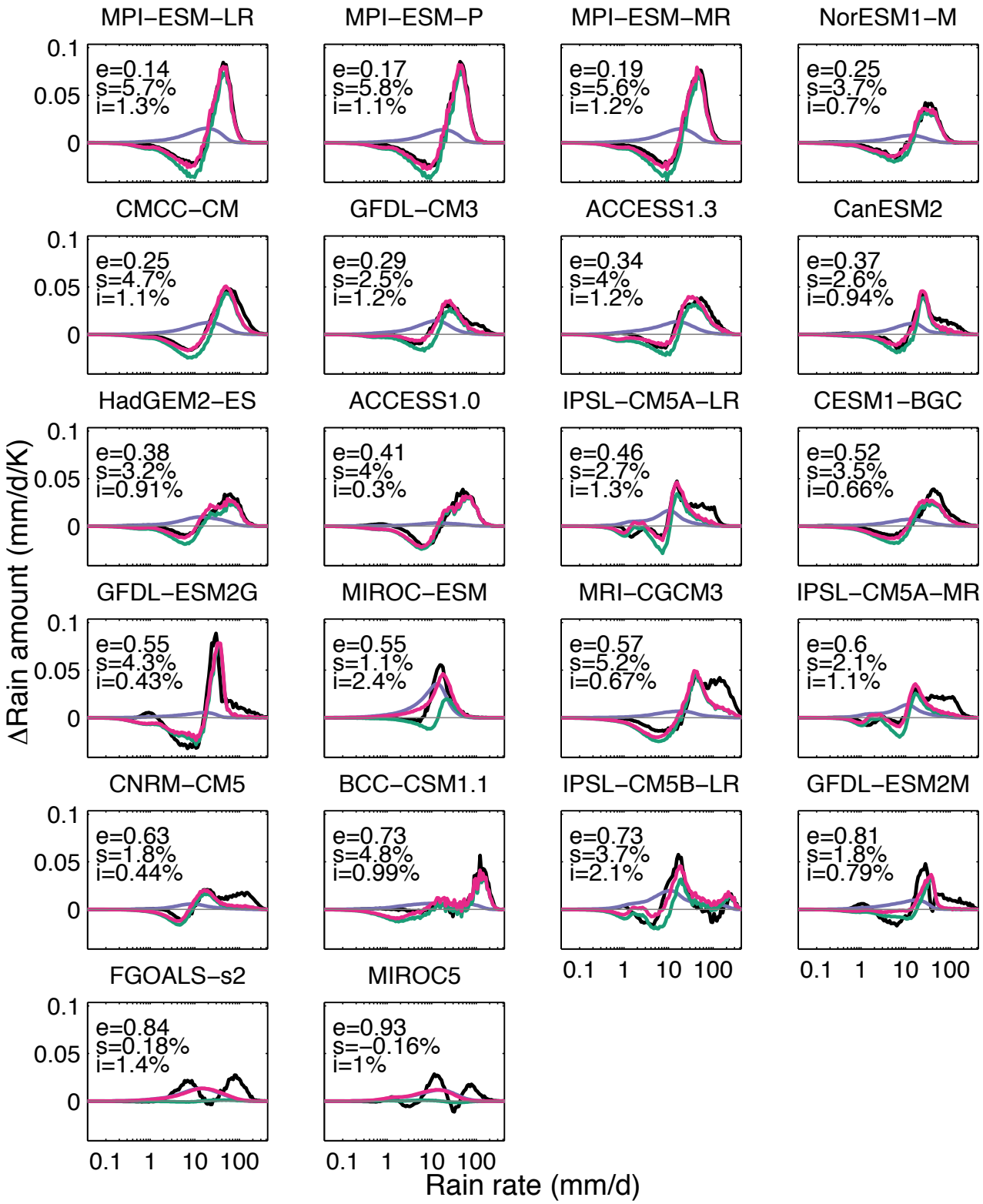

FIG. S1. Rain amount response to CO_2 doubling for each CMIP5 model and its shift, increase, and shift-plus-increase fit. At top left error (e), shift (s) and increase (i) are listed. Models are ordered from smallest to largest error.

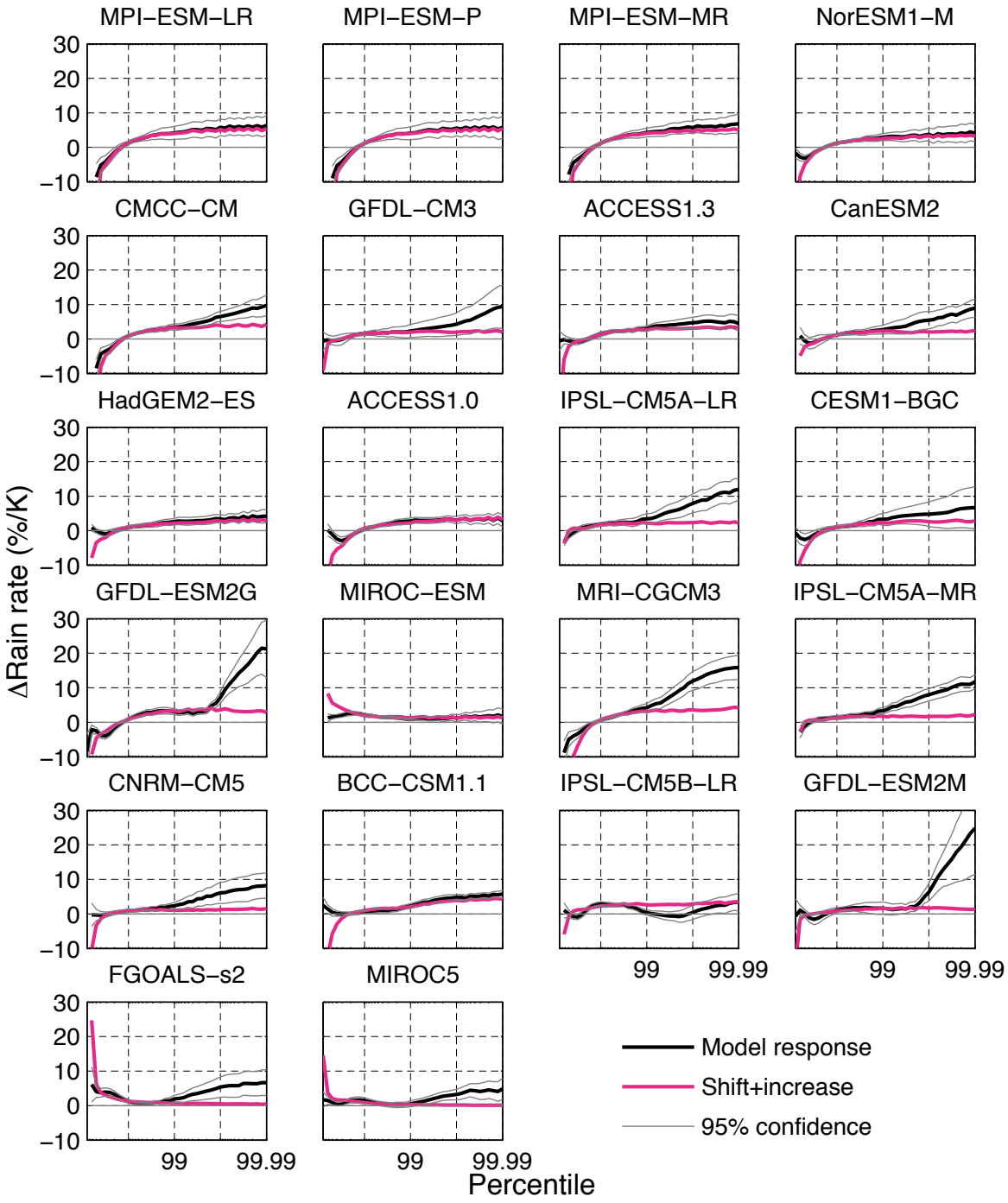

FIG. S2. Extreme precipitation response (% K^{-1}) to CO_2 doubling in each CMIP5 model (black) and its shift-plus-increase (magenta).

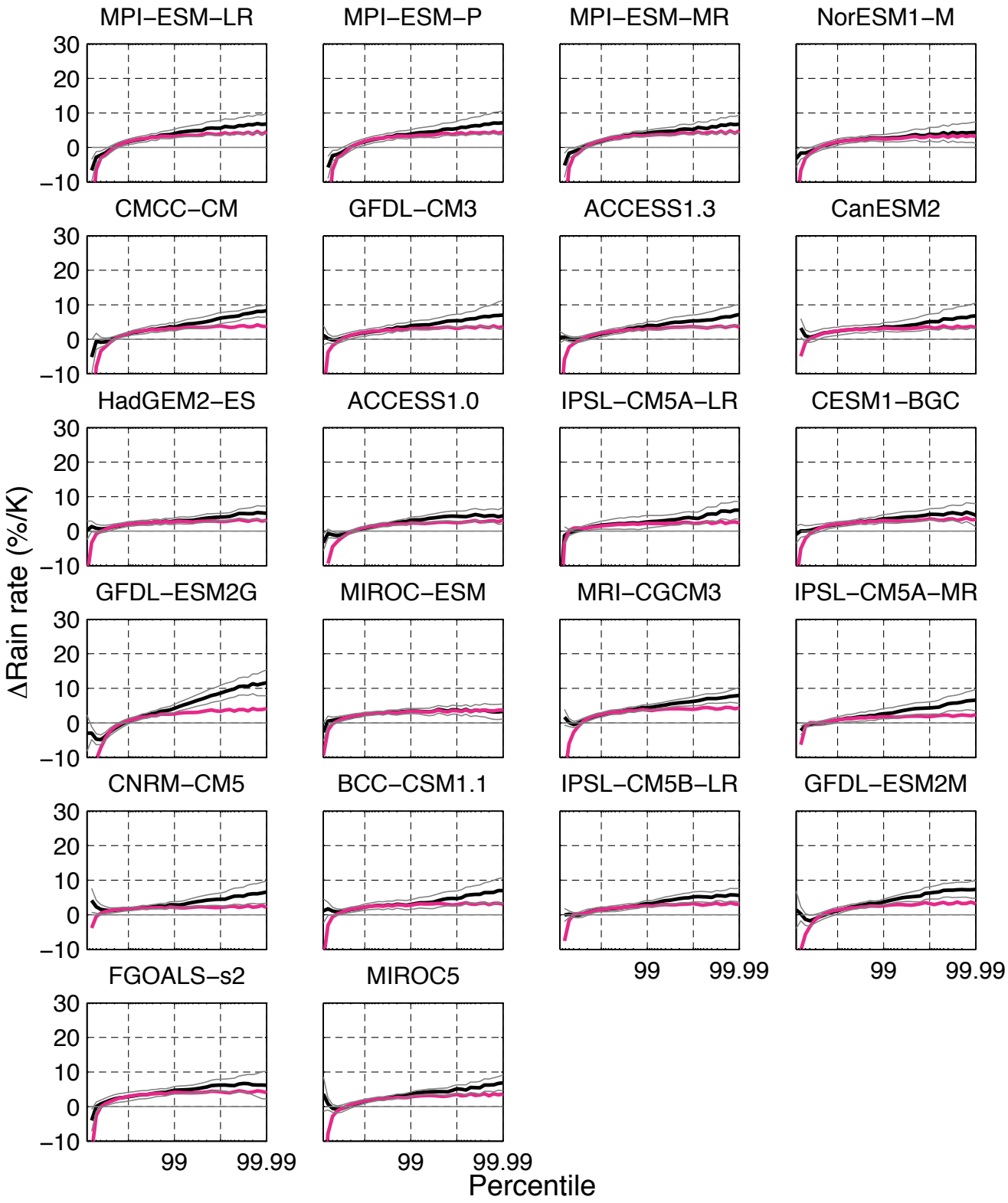

FIG. S3. Extra-tropical extreme precipitation response (% K^{-1}) to CO_2 doubling in each CMIP5 model (black) and its shift-plus-increase (magenta).

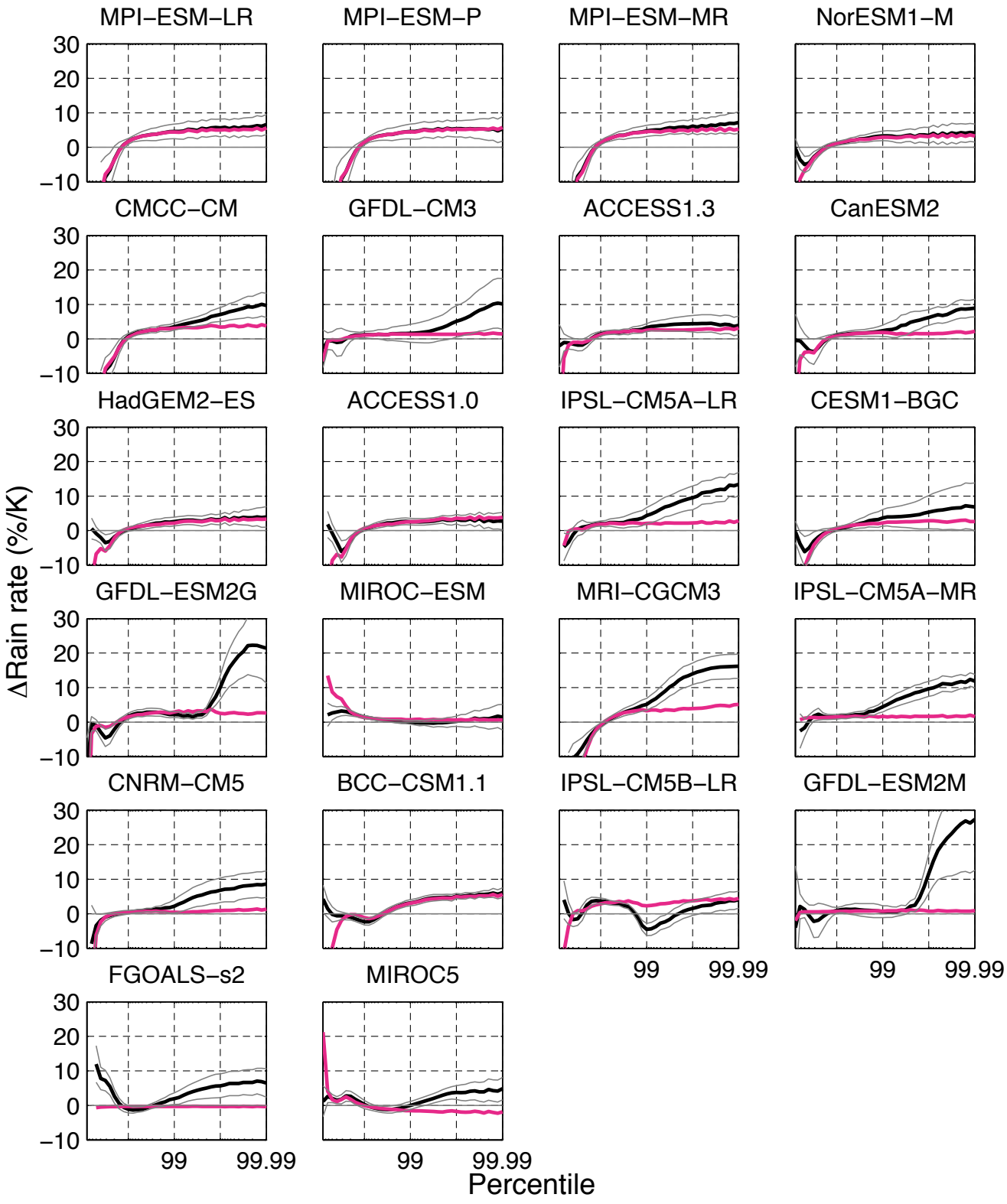

FIG. S4. Tropical extreme precipitation response (% K^{-1}) to CO_2 doubling in each CMIP5 model (black) and its shift-plus-increase (magenta).

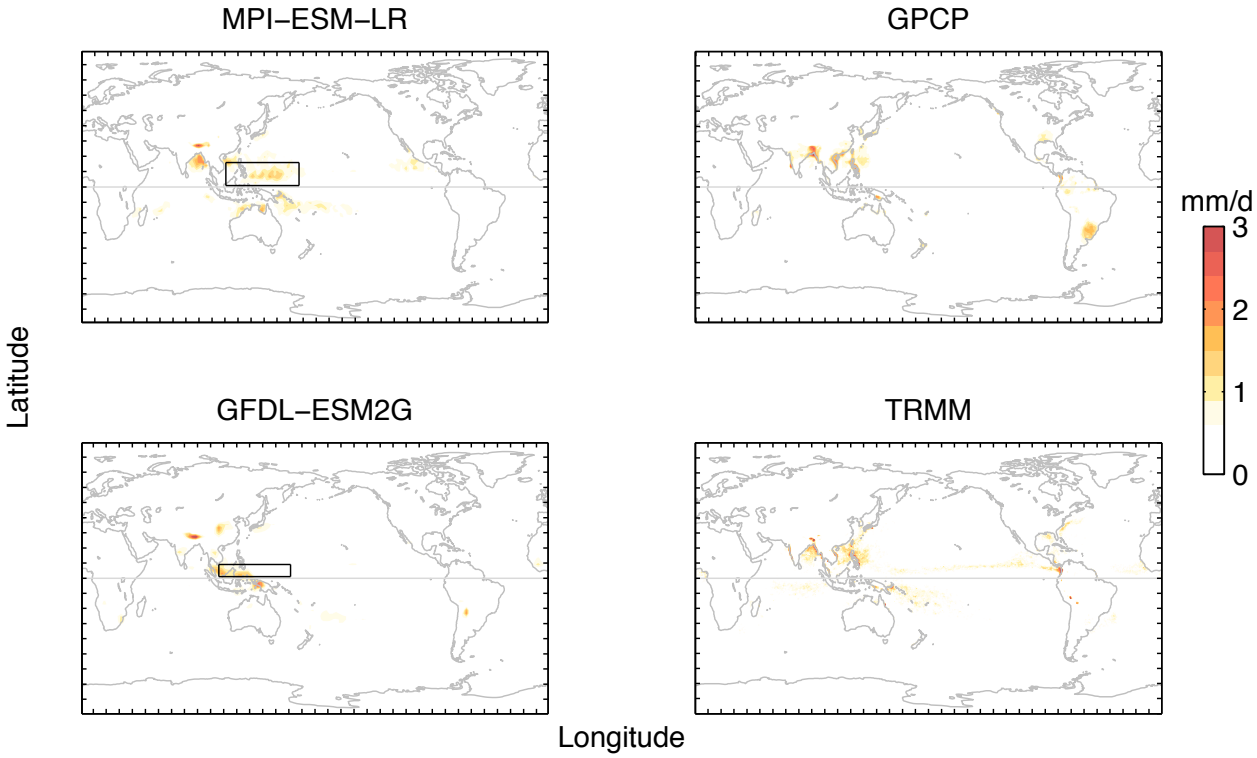

FIG. S5. Maps of the rain amount (mm d^{-1}) falling in the top 0.1% of events from the first ten years of the RCP8.5 scenario in MPI-ESM-LR (top left) and GFDL-ESM2G (bottom left) model simulations and GPCP (top right) and TRMM 3B42 (bottom right) observations. Boxes for each model show the subdomain in Figures S6 and S7.

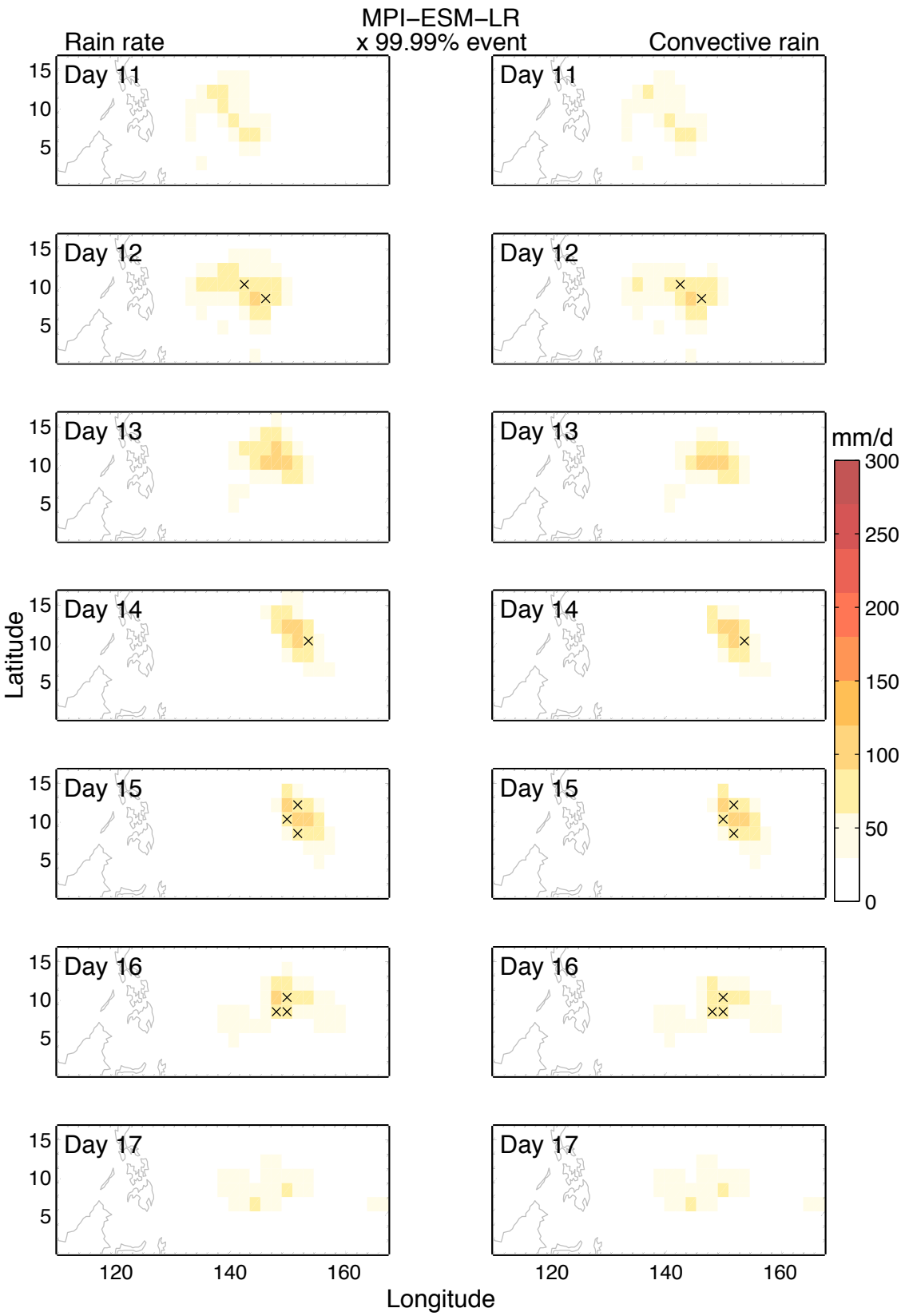

FIG. S6. Rain rate and convective rain (mm d^{-1}) for a 99.99th percentile event in the MPI-ESM-LR model chosen from the first ten years of the RCP8.5 simulation.

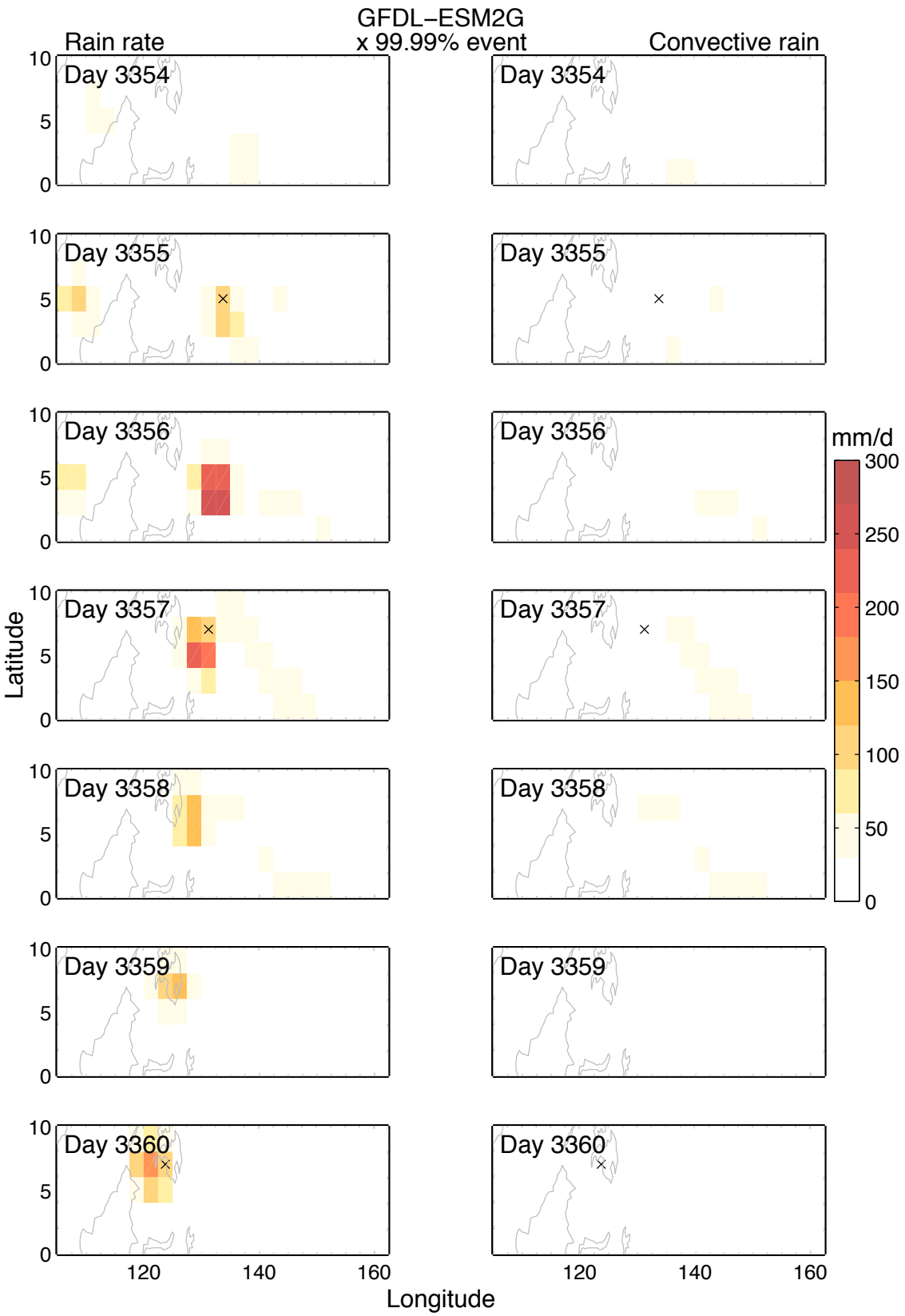

FIG. S7. Rain rate and convective rain (mm d^{-1}) for a 99.99th percentile event in the GFDL-ESM2G model chosen from the first ten years of the RCP8.5 simulation.

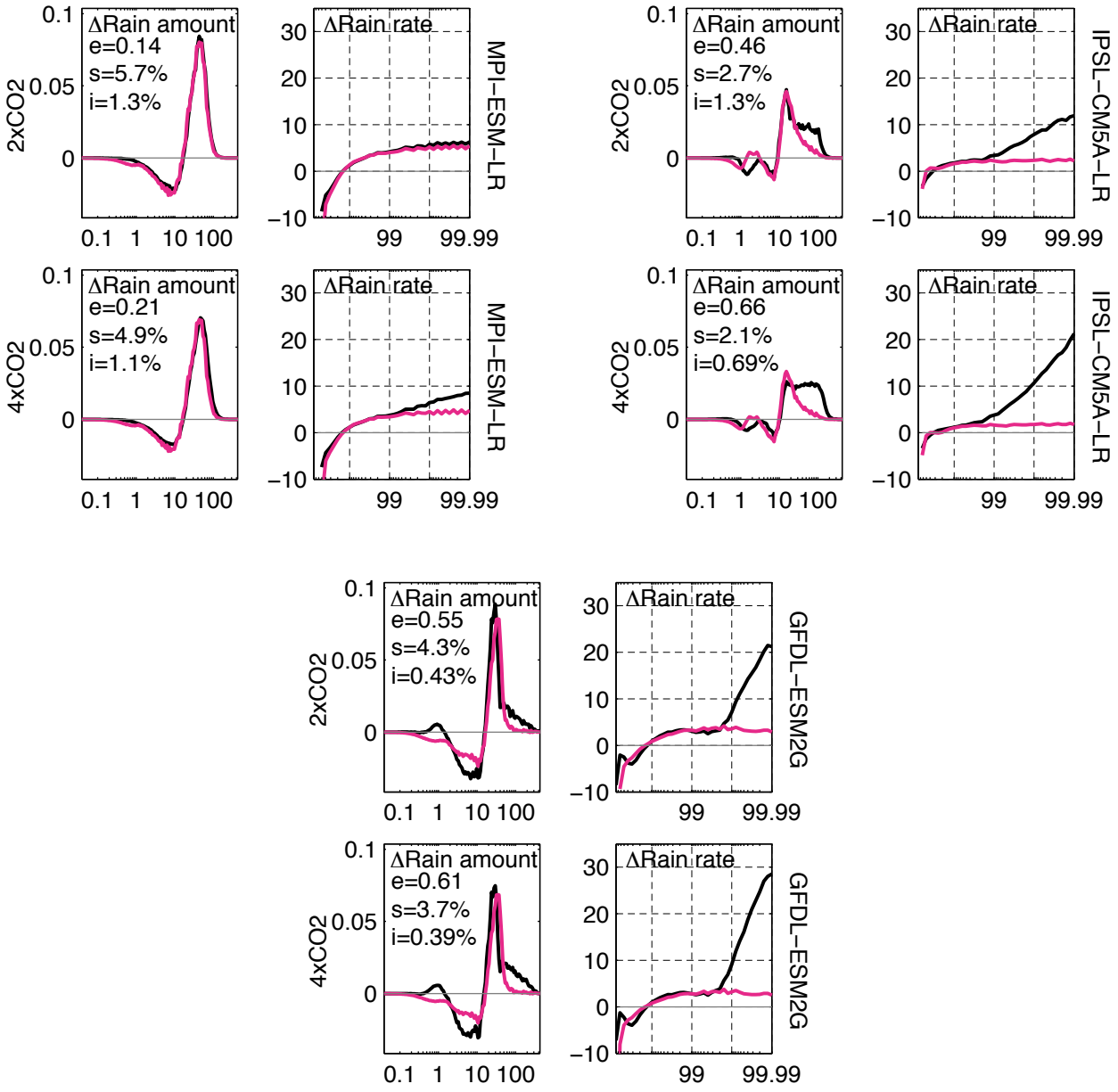

FIG. S8. MPI-ESM-LR (top left), IPSL-CM5A-LR (top right), and GFDL-ESM2G (bottom) models 2x (top) and 4xCO_2 (bottom) rain amount (left) and extreme rain rate (right) responses. Model response (black) and shift-plus-increase (magenta). Error e, shift s, and increase i are noted in the top left of the rain amount response panels.